Journal of Coordination Chemistry

ISSN: 0095-8972 (Print) 1029-0389 (Online) Journal homepage: http://www.tandfonline.com/loi/gcoo20

Towards tuning PDT relevant photosensitizer properties: comparative study for the free and Zn^{2+} coordinated meso-tetrakis[2,6-difluoro-5-(N-methylsulfamylo)phenyl]porphyrin

Janusz M. Dąbrowski, Barbara Pucelik, Mariette M. Pereira, Luis G. Arnaut & Grażyna Stochel

To cite this article: Janusz M. Dąbrowski, Barbara Pucelik, Mariette M. Pereira, Luis G. Arnaut & Grażyna Stochel (2015) Towards tuning PDT relevant photosensitizer properties: comparative study for the free and Zn^{2+} coordinated meso-tetrakis[2,6-difluoro-5-(N-methylsulfamylo)phenyl]porphyrin, Journal of Coordination Chemistry, 68:17-18, 3116-3134, DOI: 10.1080/00958972.2015.1073723

To link to this article: http://dx.doi.org/10.1080/00958972.2015.1073723

Journal of Coordination Chemistry, 2015
Vol. 68, Nos. 17–18, 3116–3134, http://dx.doi.org/10.1080/00958972.2015.1073723

Towards tuning PDT relevant photosensitizer properties: comparative study for the free and Zn^{2+} coordinated *meso*-tetrakis[2,6-difluoro-5-(*N*-methylsulfamylo) phenyl]porphyrin

JANUSZ M. DĄBROWSKI*†, BARBARA PUCELIK†, MARIETTE M. PEREIRA‡, LUIS G. ARNAUT‡§ and GRAŻYNA STOCHEL*†

†Faculty of Chemistry, Jagiellonian University, Kraków, Poland
‡Chemistry Department, University of Coimbra, Coimbra, Portugal
§Luzitin SA, Coimbra, Portugal

(*Received 14 April 2015; accepted 10 July 2015*)

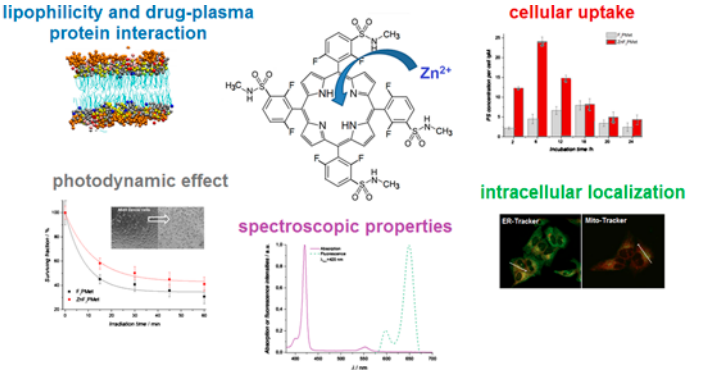

The spectroscopic, photochemical, and biological studies of 5,10,15,20-tetrakis[2,6-difluoro-5(*N*-methylsulfamylo)phenyl]porphyrinate Zn(II) (ZnF_2PMet) were carried out including absorption and fluorescence spectra, fluorescence quantum yields, triplet absorption spectra, triplet lifetimes, singlet oxygen quantum yield, and reactive oxygen species (ROS) detection under biological conditions and compared with its free-base analog (F_2PMet). Zinc coordination into the porphyrin ring results in decrease of hydrophobicity and in higher cellular uptake. F_2PMet localized specifically in endoplasmic reticulum and mitochondria while the ZnF_2PMet is more diffused all over the cell, bonded to membrane proteins, as assessed by fluorescence microscopy. Zn-porphyrin exhibits greater singlet oxygen quantum yield than its free-base analog. Studies with fluorescent probes confirm that the ZnF_2PMet produces mostly singlet oxygen, whereas F_2PMet generates more hydroxyl radicals as the ROS. F_2PMet is a more effective photosensitizer *in vitro* than its zinc complex, thus, the final photodynamic effect depends more on the nature of ROS than on the higher cellular uptake.

Keywords: Metalloporphyrins; Zn(II) complexes; Photodynamic therapy; Singlet oxygen; Hydroxyl radicals

*Corresponding authors. Email: jdabrows@chemia.uj.edu.pl (J.M. Dąbrowski); stochel@chemia.uj.edu.pl (G. Stochel)
Dedicated to Professor Rudi van Eldik on the occasion of his 70th birthday.

1. Introduction

Photodynamic therapy (PDT) has emerged as a promising, noninvasive treatment modality of cancer. PDT involves administration of the photochemically active substance (photosensitizer) into the organism and its excitation with visible or NIR light. In consequence, a cascade of photochemical reactions is induced (photodynamic effect), which leads to apoptosis, necrosis or autophagy of cancer cells, shutting down the tumor microvasculature, and eventually activation of antitumor immune response [1]. Photodynamic effect has also been applied in microbiology, particularly in photoinactivation of drug-resistant pathogens [2, 3].

Most of the photosensitizers investigated for PDT are porphyrins [4–8], chlorins [9–13], bacteriochlorins [14–22], and phthalocyanines [23–26]. They strongly absorb light within the phototherapeutic window (630–850 nm) and generate singlet oxygen and/or other oxygen-centered radicals with high quantum yields [27]. In the majority of porphyrin- and phthalocyanine-based photosensitizers, type-II mechanism (energy transfer from the excited photosensitizer to molecular oxygen) with efficient singlet oxygen generation is dominant [8, 9, 23]. However, the type-I reactions (triplet–triplet annihilation or electron transfer reactions involving T_1 state of the photosensitizer with generation of radical intermediates) were shown to be the most exclusive way of reactive oxygen species (ROS) generation (superoxide ion and hydroxyl radicals) by Pd-bacteriopheophorbide [28]. Moreover, the combined effects with the formation of both singlet oxygen and free radicals accompanied with enhanced photodynamic effect have been recently described [14–16, 29, 30].

The size of typical cells is 10–30-μm diameter and the diffusion distance of singlet oxygen in a cell is ca. 550 nm, and that of $OH^{\cdot}$ radicals is even smaller [31]. Taking this into account and the short lifetime of singlet oxygen (10^{-6}–10^{-9} s) [32], it is obvious that only cellular targets that are close to the site of ROS formation are destroyed by photodynamic effect. Thus, the nature of such targets and the extent of photodamage have a great impact on the PDT outcome. The cellular uptake and subcellular distribution depend on the charge, lipophilicity, and structure of the photosensitizer. Hydrophobic photosensitizers localize in the cytoplasmic, mitochondrial and lysosomal membranes, in the Golgi apparatus and endoplasmic reticulum (ER) [33]. Hydrophilic photosensitizers that are too polar to cross the plasma membrane are typically internalized by endocytosis and are primarily localized in lysosomes [34]. The accumulation of the photosensitizers in organelles such as mitochondria and ER is more efficient in killing cells upon illumination than accumulation in other cellular targets [14, 30, 35–37].

In the case of many tetrapyrrolic photosensitizers, metallation is a promising approach to change the electrochemical, spectroscopic, photochemical, and photophysical properties of photosensitizers in the context of their use in phototherapy [27, 38], solar energy conversion [27, 39], and in biomimetic catalysis [40, 41]. In this way their hydrophobicity/hydrophilicity, degree of aggregation, stability, and consequently the cellular uptake and intracellular localization can also be modulated [42]. Since aggregation of photosensitizers causes a shortening of the triplet lifetime and a reduction of photosensitizing efficiency [43], the presence of ions, which can give octahedral hybrid orbitals, guarantees a reasonable yield of $^1O_2$ generation because axial ligands may generate steric hindrance to intermolecular aggregation. However, there are several reports claiming that the presence of Zn(II) can still be problematic from an aggregation standpoint. For example, Zn(II) phthalocyanines often show aggregation effects in polar solvents [44, 45] and very strongly basic axial ligands are usually required to overcome this problem. Our approach is to introduce electron

withdrawing halogens in the *ortho* position of the phenyl groups of the macrocycle in an attempt to overcome the problem of aggregation. Our earlier studies with other halogenated porphyrins established that the presence of bulky *orthochloro* groups reduce the tendency of porphyrins to aggregate [6].

In this work, we describe and compare the chemical and photophysical properties of *meso*-substituted halogenated sulfonamide porphyrin (F_2PMet) with its zinc-chelated derivative (ZnF_2PMet). Their chemical structures are illustrated in chart 1.

The selection of these fluorinated sulfonamide tetraphenylporphyrins are based on the hypothesis that they should be more photostable and more lipophilic than their sulfonated or sulfoester analogs previously described [6, 7]. Moreover, they should permeate the cell membrane better, localize in the ER or in the mitochondria, and produce larger amounts of ROS before bleaching. These properties should lead to higher PDT efficacy than that recently presented for halogenated sulfonated porphyrins. The expectation of an enhanced phototoxicity motivated this investigation of the *in vitro* photodynamic effect of fluorinated sulfonamide tetraphenylporphyrins and its relation to intracellular localization, and to the nature of the ROS generated.

The mechanistic insights have shown that F_2PMet can produce oxygen-centered radicals as well as singlet oxygen and in contrast, ZnF_2PMet generates exclusively singlet oxygen. Their photogeneration in various ROS was monitored by aminophenyl fluorescein (APF), hydroxyphenyl fluorescein (HPF), and singlet oxygen sensor green (SOSG) fluorescence probes in order to highlight the relative contribution of each ROS to photodynamic efficacy. The spectroscopic and photochemical studies were carried out to understand and explain not only the mechanisms of photochemical processes of these compounds, but also the biological consequences such as photodynamic efficacy, which are based on generation of various ROS. The PDT efficacy of F_2PMet and ZnF_2PMet was examined on human adenocarcinoma cells (A549). The effects of zinc insertion on the hydrophilicity, cellular uptake, and photodynamic activity were examined. These studies may contribute to the choice of optimal photoactive compounds for specific applications. Free-base sensitizers that generate simultaneously singlet oxygen and hydroxyl radicals are probably a better choice for PDT. On the other hand, zinc porphyrins or bacteriochlorins that generate mostly singlet oxygen with the high quantum yields should be more efficient in the photodynamic inactivation of pathogens [2, 3].

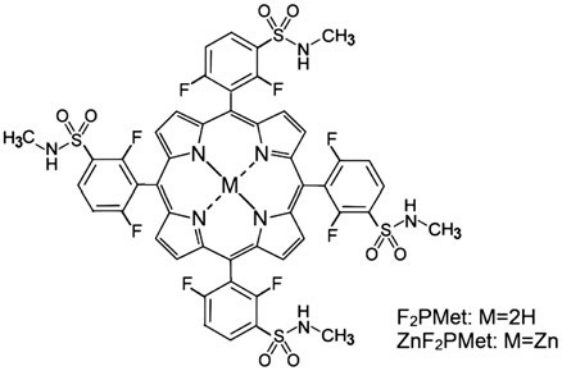

Chart 1. Chemical structure of free-base halogenated sulfonamide porphyrin (F_2PMet, M=2H) and its metal complex (ZnF_2PMet, M=Zn).

2. Experimental

2.1. *Chemicals*

All chemicals were of reagent grade and used as received. 5,10,15,20-Tetrakis[2,6-difluoro-5-(*N*-methylsulfamylo)phenyl]porphyrin (F_2PMet) was synthesized via recent optimizations of the nitrobenzene method [46, 47] and basic properties were recently published [14]. 5,10,15,20-Tetrakis[2,6-difluoro-5-(*N*-methylsulfamylo)phenyl]porphyrinate Zn(II) was prepared according to the method of Adler and co-workers [48].

Media for cell culture [Dulbecco's Modified Eagle's Medium (DMEM)] and PBS (phosphate buffer saline) were from Biomed (Poland). Triton X-100 was from POCH (Poland). Solvents used in all experiments, [3-(4,5-dimethylthiazol-2-yl)-2,5-diphenyl tetrazolium bromide] (MTT), albumin from human serum (HSA), penicillin, streptomycin, 3′-(*p*-aminophenyl)fluorescein (APF), and 3′-(*p*-(hydroxyphenyl)fluorescein (HPF), were purchased from Sigma-Aldrich. Singlet oxygen sensor green® (SOSG) was obtained from Invitrogen.

2.2. *Spectroscopic and photophysical experiments*

UV/vis absorption spectra were recorded with a Hewlett Packard HP8453 spectrophotometer. Solutions containing samples of photosensitizers were dissolved in ethanol in quartz cuvettes. Fluorescence measurements were made in 1-cm quartz cuvettes in ethanol solutions, carefully deaerated by saturating with N_2 for 15 min. The *meso*-Tetraphenylporphyrin (TPP) in toluene was used as a fluorescence standard ($\Phi_F = 0.11$) for determination of the fluorescence quantum yields of all studied compounds. Φ_F was calculated by comparing integrated emission of the sample to that of the reference solution, taking into account the difference in refractive indices of the solvents ($\eta_{EtOH} = 1.36242$; $\eta_{toluene} = 1.49693$) [9].

The triplet state lifetimes were obtained with an Applied Photophysics LKS.60 flash photolysis spectrometer. The kinetic curves of the transient absorption of TPP, ZnTPP, F_2PMet, and ZnF_2PMet within the range of 300–700 nm were recorded after laser excitation ($\lambda = 355$ nm, $E_{max} = 100$ mJ/pulse, and full width at half maximum FWHM = 6 ns). At least ten kinetic runs were registered for each set of conditions and the mean value was taken for further calculations. The measurements were done at 20 °C. All solutions of photosensitizers were freshly prepared before the measurements. Their absorbance at 355 nm was ca. 0.2. The stability of the samples was confirmed by comparing their absorption spectra before and after each flash photolysis experiment. The samples showed less than 5% degradation after 1000 laser flashes at 355 nm. The photolysis experiments run in the presence of oxygen involved saturation of the solutions with air at 20 °C prior to the measurements. For experiments in the absence of oxygen, the solutions were purged with argon for 15 min until no change in the decay rate was observed, and were kept under argon during the measurements. Transient absorption decay was collected at 460 nm from the triplet absorption spectra.

Quantum yields of singlet oxygen generation in ethanol were determined using a procedure described in detail elsewhere [49], with phenalenone as a reference, for which $\Phi_\Delta = 0.95$ in ethanol. Singlet molecular oxygen phosphorescence at 1270 nm was detected at room temperature following laser excitation of ethanol solutions containing the sensitizer at concentration related to the absorbance of 0.2 in 1-cm quartz cuvette at the excitation wavelength. The excitation of the samples at 355 nm (the third harmonic of a Nd–YAG

laser Spectra-Physics Quanta-Ray GRC-130) was used as usual, but the flash photolysis equipment was modified to allow for luminescence detection at 800–1400 nm. The emission was filtered by a Melles Griot dielectric mirror reflecting more than 99.5% of the incident light at 610–860 nm and by a Scotch RG665 filter. The infrared emission transmitted by these filters was split by a monochromator with a 600 lines/cm grading mounted in the place of the usual UV/vis grading. The wavelength of 1270 nm was selected for detection in a Hamamatsu R5509-42 photomultiplier, cooled to 193 K in a liquid nitrogen chamber.

2.3. *Detection of ROS in solution*

The 3′-(*p*-aminophenyl)fluorescein (APF) and 3′-(*p*-hydroxyphenyl)fluorescein – selective probes for hydroxyl radicals and singlet oxygen sensor green® (SOSG) – specific probe for singlet oxygen were employed for detection of ROS formation during illumination. Photosensitizer solutions were diluted to a final concentration of 5 μM per well in PBS. Next, the fluorescent probe SOSG or APF was added to each well at a final concentration of 10 μM. Photosensitizer solutions were irradiated with the 595 ± 20-nm laser diode light with power of 1.7 mW and light was delivered for various time intervals. The microplate reader (Tecan Infinite M200 Reader) was used for acquisition of fluorescence signal immediately before and after illumination. When APF and HPF were employed, fluorescence emission at 515 nm was measured upon excitation at 492 nm. With SOSG, the corresponding values were 525 and 505 nm, respectively.

2.4. *n-Octanol/water partition coefficients and photosensitizer binding to serum albumin determined by fluorescence measurements*

The *n*-octanol/PBS partition coefficients were measured following the shake-flask method with minor modification to determine the equilibrium concentration of F_2PMet and ZnF_2PMet in *n*-octanol and PBS mixed in equal volumes. The sulfonamide halogenated (metallo)porphyrin ($\sim 5 \times 10^{-2}$ μmol) was dissolved in 5 mL of *n*-octanol previously saturated with a solution of PBS. The same volume of PBS saturated with *n*-octanol was added and mixed on a vortex device for 10 min and then the phases were separated by centrifugation at 3700 rpm for 2 min. A 0.02 mL of the PBS/*n*-octanol phase was taken and diluted with DMSO to obtain 0.5% of PBS/*n*-octanol content in the DMSO final solution. This solution was left for 5 min in the ultrasonic bath. The fluorescence of each DMSO/*n*-octanol and DMSO/PBS solution was measured using fluorescence spectrometer LS 55 (Perkin Elmer) and compared with calibration curve to obtain the concentration of the photosensitizer. The photosensitizers were excited at the Soret absorption band (at 410 nm for F_2PMet and 420 nm for ZnF_2PMet) and the fluorescence spectra were collected in the region between 550 and 780 nm. The partition coefficients were calculated from the ratio c_{oct}/c_{PBS}, where c_{oct} and c_{PBS} are the concentrations of the porphyrins in *n*-octanol and in PBS, respectively.

The fluorescence intensities were recorded with a Perkin Elmer Fluorescence Spectrometer LS 55. Samples of human serum albumin (HSA) (5 μM) were titrated in the quartz cell by successive additions of both porphyrin solutions. Next, the photosensitizer solution was added into HSA to give a final concentration in the range 1–40 μM. Fluorescence emission spectra were recorded from 300 to 400 nm with excitation at 295 nm. The excitation and emission slits were both set to 10 nm and scanning speed to 50 nm min^{-1}. All experiments were carried out at room temperature.

2.5. *Biological* in vitro *studies*

The A549 (human lung adenocarcinoma) cells were seeded into a 96-well culture plate in a DMEM supplemented with 10% fetal bovine serum (FBS) and antibiotics. Cells were kept at 37 °C in a 95% atmospheric air and 5% CO_2 humidified atmosphere for 24 h.

2.5.1. Light source. Light system and LED illuminator (Photon Institute, Krakow, Poland), and sample chamber with stabilized temperature and the display was employed for illumination of plate with seeded cells. The diode (595 nm ± 20 nm) was adjusted to give a uniform spot of irradiated area with a fluence rate of 1.7 mW as measured with a power meter (Light Engine UNO 50) and to excite the same number of molecules of F_2PMet and ZnF_2PMet.

2.5.2. Cellular uptake. Cells were prepared as described above. After 24 h, the cells were incubated in 37 °C with concentrations at 5 μM of F_2PMet and ZnF_2PMet for various time intervals from 1 to 24 h. The solutions of photosensitizers were prepared by diluting the porphyrin stock solution in DMSO with the culture medium to the desired final concentration. The highest concentration of DMSO in medium did not exceed 0.5%. After incubation, the cells were washed twice with PBS and solubilized in 30 μL of Triton X-100 and 70 μL of DMSO/ethanol solution (1 : 3). The retention of cell-associated porphyrin was detected by fluorescence measurement with the microplate reader (Tecan Infinite M200 Reader).

2.5.3. Cytotoxicity and cell survival assay. The MTT [3-(4,5-dimethylthiazol-2-yl)-2,5-diphenyl tetrazolium bromide] assay for measuring cell survival has been used successfully to quantitate photosensitizer-mediated cytotoxicity. For each experiment, two identical 96-well plates with A549 cell culture were used. After cell attachment, a photosensitizer solution in growth medium (DMSO < 0.5%) at concentrations which varied from 0.5 to 200 μM was added to the culture. Treated cultures were incubated for 6 h or 24 h with F_2PMet and ZnF_2PMet at 37 °C in the dark. Next, the photosensitizer solution of each well was removed, cells were washed in PBS and 200-μL fresh culture medium supplemented with FBS and antibiotics was added to each well and cells were returned to the incubator for 24 h. MTT was dissolved at 5 mg mL^{-1} in PBS. Briefly, 22 μL of MTT solution was added to each well (final concentration 0.5 mg mL^{-1}) and the microplates were further incubated for 3 h. Medium was then discarded and 100 μL of mixture of DMSO/methanol (1 : 1) was added to the cultures and mixed thoroughly to dissolve the dark blue crystals of formazan. Formazan quantification was performed using an automatic microplate reader (Tecan Infinite M200 Reader) by absorbance measurements with a 565 nm test wavelength. Each experiment was repeated three times. Data were expressed as mean absorbance value of six samples and standard error of the mean.

2.5.4. Photodynamic effect experiments. On the basis of cytotoxicity results, nontoxic concentration (5 μM) was selected. The porphyrins (F_2PMet and ZnF_2PMet) were dissolved in DMSO and stored in the dark. The A549 cells were incubated for 24 h at 37 °C. After being washed with fresh medium the cells were incubated in the dark with 5 μM

photosensitizer solution in a culture medium for 6 h. The highest DMSO concentration in the medium was less than 0.5%. After this incubation the cells were washed with PBS buffer and illuminated with the 595 ± 20 nm laser diode light with fluence rate of 1.7 mW for various time intervals. The light spot covered 12 wells, which were considered as one experimental group illuminated in the same time. Next, the cells were washed with fresh medium and plates were returned to the incubator for 24 h (37 °C, 5% CO_2). Cell viability was determined by a MTT assay performed 24 h after irradiation. Data were expressed as percentage of cell survival with reference to control cells with no treatment of photosensitizer and without illumination. Each experiment was repeated three times.

2.5.5. Intracellular distribution. The intracellular distribution of F_2PMet was assessed in A549 cell line. A549 cells were plated at a density of 15×10^3 cells per well in eight-well slides (IBIDI, Germany) and were kept at 37 °C in a 95% atmospheric air and 5% CO_2 humidified atmosphere for 24 h. After being washed with fresh medium, the cells were incubated in the dark with 5 μM sensitizers, diluted in cell medium for ca. 18 h, at 37 °C in a CO_2 incubator (5% (v/v) CO_2 in air). After being washed with HBSS/Hepes buffer, the cells were incubated with specific intracellular organelle probes: 100 nM of Mito-tracker green, 1 mM ER-Tracker green, 75 nM Lyso-Tracker green (Molecular Probes, Invitrogen Life Technologies), diluted in HBSS/HEPES buffer. After ~30 min incubation, at 37 °C in the dark, the cells were washed with HBSS/HEPES buffer and the slide was transferred to the microscope stage. Cells were visualized under a confocal microscope (LSM 510 Meta; Carl Zeiss, Jena, Germany) with a 63× oil immersion objective (Plan-Apochromat, 1.4 NA; Carl Zeiss). Images from the porphyrin and bacteriochlorin were obtained by exciting at 514 nm using an argon laser (45 mW) and fluorescence was detected after passing through a long-pass filter 575 and 700 nm, respectively. To obtain the fluorescence profile of the fluorescence probes a helium–neon laser (5 mW) was used as light source at 633 nm for visualization of cell morphology.

3. Results

3.1. *Spectroscopic properties of the studied sensitizers*

The absorption spectra of the studied compounds are typical for porphyrins and their metal complexes. Electronic absorption spectrum of F_2PMet shows the five characteristic bands originated from free-base porphyrins with the D_{2h} symmetry, described by four orbitals model [50]. The intense Soret band is observed at 410 nm, Q_x, Q_y, and two additional bands are observed at 505, 537, 581, and 639 nm, respectively (table 1). These bands in the visible part of the spectrum are due to vibrational coupling effects and originate from HOMO (b_{1u} orbital) to the first vibrationally excited state of LUMO (b_{2g} orbital) or to LUMO + 1 (b_{3g} orbital) transitions. In ZnF_2PMet absorption spectrum, a red shifted Soret band and two Q bands are observed (figure 1). Introduction of Zn in the center of tetrapyrrolic ring change the symmetry of the free-base porphyrin from D_{2h} to D_{4h}. According to Gouterman's four-orbitals model, formation of metalloporphyrin enforces the degeneracy of the two molecular orbitals: LUMO and LUMO − 1 and the absorption spectra show only two Q bands. The fourfold rotational symmetry of ZnF_2PMet is also reflected in the

Table 1. Spectroscopic properties of fluorinated porphyrin and its zinc complex in ethanol.

Porphyrin	Absorption λ (nm), ε (M^{-1} cm^{-1}) × 10^3					Fluorescence λ (nm)	Φ_F	logP_{OW}
F_2PMet	*B*	Q_y(0–1)	Q_y(0–0)	Q_x(0–1)	Q_x(0–0)	(0–0) (1–0)		
	410 379	537	505 25	582 7.7	639 0.7	652 731	0.05	2.84
ZnF_2PMet	*B*	Q_{xy}(0–1)	Q_{xy}(1–0)					
	420 496	588 16.8	549			599 651	0.001	1.72

coincidence of the $-x$ and $-y$ components of the Q bands (Q_{xy}) and may result in enhancement of the molar absorption coefficient values, while the lower symmetry of the free-base porphyrin is indicated by the splitting of the Q bands into Q_x and Q_y.

The absorption maxima and the molar absorption coefficient values are listed in table 1. Because of the interaction between the central zinc and the π-conjugate system, the Q bands of the zinc porphyrin are characterized by higher values of molar absorption coefficients than the metal-free analog. The fluorescence spectra of F_2PMet and ZnF_2PMet have two maxima [652 nm, 731 nm for F_2PMet and 599, 651 for ZnF_2PMet (figure 1, table 1)]. Fluorescence spectra of zinc porphyrin is blue shifted when compared with the emission of its respective free-base analog. The fluorescence excitation spectra of investigated compounds correspond well with their absorption spectra and confirm the purity and non-aggregation of the samples. The fluorescence quantum yields obtained for studied porphyrins are also presented in table 1. The free-base porphyrin and its zinc derivative exhibit low fluorescence

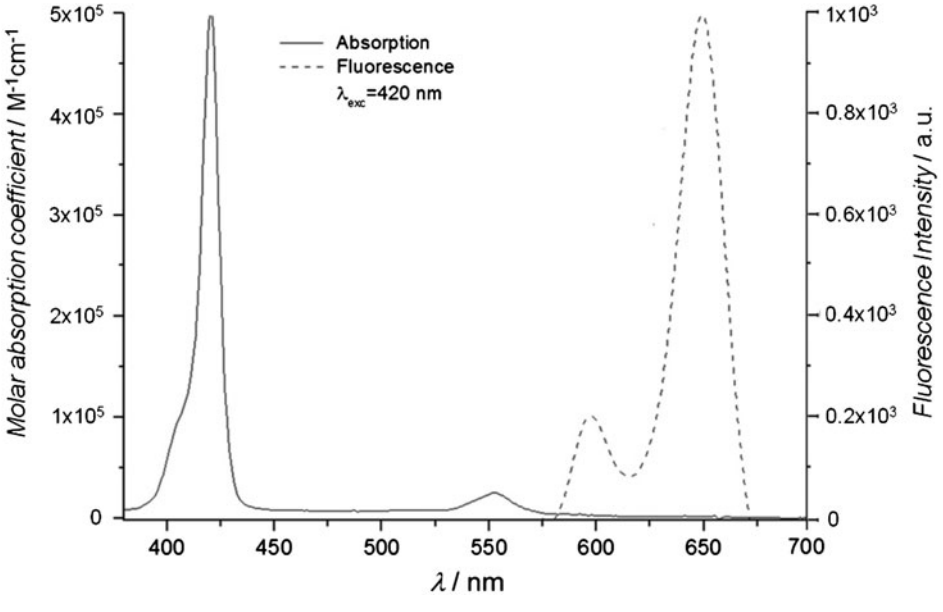

Figure 1. Electronic absorption and fluorescence spectra of ZnF_2PMet measured in ethanol at room temperature.

quantum yields. The fluorescence quantum yield determined for F_2PMet is reduced by a factor of two compared to TPP. A further decrease in Φ_F is observed for ZnF_2PMet ($\Phi_F = 0.001$). This is consistent with the internal heavy atom effect, discussed below. It is not surprising since metalloporphyrins with closed metal shells are less fluorescent than the corresponding free bases. Moreover, they have shorter fluorescence lifetimes and higher efficiencies of intersystem crossing to the triplet state promoted by the spin-orbit coupling mechanism. Low fluorescence quantum yields obtained for both fluorinated porphyrins reported in this work suggest that intersystem crossing to the triplet state is also a major singlet deactivation pathway for these molecules.

3.2. *n-Octanol: water partition coefficients*

Partition coefficients in *n*-octanol:water (1 : 1, v : v), P_{OW}, are a convenient measure of a drug's polarity and an indication of its ability to cross cell membranes. For drug delivery, the lipophilic/hydrophilic balance has been shown to be a contributing factor for the rate and extent of drug absorption. Since biological membranes are lipoidal in nature, the rate of drug transfer for passively absorbed drugs is directly related to the lipophilicity of the molecule. We have determined P_{OW} using a minor modification of the shake-flask method [51] recently described by us [52], and presented in table 1. The photosensitizers studied in this work have different solubility. Interestingly, zinc insertion into the porphyrin structure decreases the hydrophobicity. ZnF_2PMet is remarkably more hydrophilic ($\log P_{OW} = 1.72$) than F_2PMet. Similar studies with the set of porphyrins also have demonstrated that zinc insertion on the porphyrin core results in decreased hydrophobicity [53]. This is consistent with our results reported here.

3.3. *Photophysical properties*

Laser flash photolysis was used to construct the time-resolved transient absorption spectra and to determine the triplet state lifetimes. Spectra were constructed from data recorded for the sets of decay curves, collected with 10 nm intervals. The transient absorption decays recorded in the presence of oxygen do not depend on the detection wavelength and are typical for triplet states quantitatively transferring energy to molecular oxygen. In argon-saturated ethanol solution, the decays remain monoexponential and lifetimes increase to ca. 50 μs. Transient absorption spectrum of ZnF_2PMet in ethanol is shown in figure 2. The strong negative absorbance change originates from bleaching of the ground-state absorption, while clearly defined pseudoisosbestic points reflect the fact that all molecules return to this ground state, pointing at the photodegradation as a minor decay pathway. The rate constant of energy transfer from the triplet state of the photosensitizer to molecular oxygen (k_q) can be calculated from the triplet lifetimes in the absence (nitrogen saturated solution), τ_T^o, and in the presence of oxygen (air saturated solution), τ_T, using the relation:

$$k_q = \left(1/\tau_T - 1/\tau_T^o\right)/[O_2]$$

The oxygen concentration in ethanol, $[O_2]$, is 2.1×10^{-3} M. Since $\tau_T^o >> \tau_T$ (table 2), the actual value of τ_T^o is irrelevant to calculate the value of k_q. Triplet states of porphyrins are quenched with rate constants of $1.2–1.4 \times 10^9$ $M^{-1}s^{-1}$, similar to $k_q = 1.4 \times 10^9$ $M^{-1}s^{-1}$

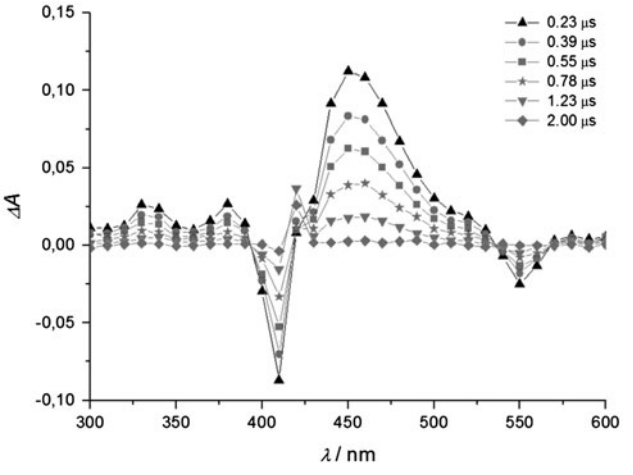

Figure 2. Time-resolved transient absorption spectra of ZnF_2PMet in ethanol, measured by laser flash photolysis; 20 °C, λ_{exc} = 355 nm.

Table 2. Triplet state lifetimes in the presence and absence of oxygen determined in ethanol, with respective oxygen quenching rate constants at room temperature and singlet oxygen quantum yields upon 355 nm excitation (Φ_Δ) for studied porphyrins.

Sensitizer	τ_T^o (µs)	$\tau_{T,air}$ (ns)	k_q	Φ_Δ
TPP	43	350	1.4×10^9	0.7
F_2PMet	62	391	1.17×10^9	0.71 ± 0.05
ZnF_2PMet	54	570	0.83×10^9	0.99 ± 0.06
Phenalenone	–	–	–	0.95 ± 0.07

determined for TPP. Spin statistics for the formation of singlet oxygen requires that k_q should be 1/9 of the diffusion rate constant, k_{diff}. The value of k_{diff} was estimated taking into account the oxygen concentration in air-saturated or oxygen-saturated ethanol and the fluorescence lifetime in ethanol of F_2PMet in the absence and in the presence of oxygen, measured as described elsewhere [29]. Triplet lifetimes are presented in table 2. Using the relationship presented above for singlet lifetimes determination, k_{diff} has been calculated to be 9.5×10^9 $M^{-1}s^{-1}$ in ethanol at 20 °C. The values of k_q reported in table 2 reach 1/9 k_{diff}, as in other reported compounds [14].

3.4. *Singlet oxygen quantum yields*

The photosensitizer in the triplet excited state participates in ROS generation. A good photosensitizer should exhibit high triplet lifetime and triplet quantum yield. Singlet oxygen quantum yield (Φ_Δ) is directly correlated to the photosensitizer's triplet quantum yield and in this work was measured by direct monitoring of $^1O_2$ phosphorescence at 1270 nm. Herein, direct detection of the phosphorescence peak of $^1O_2$ at 1270 nm in solution was monitored, and the corresponding singlet oxygen quantum yields (Φ_Δ) were calculated using phenalenone

as a reference ($\Phi_\Delta = 0.95$ in EtOH) (table 2). Singlet oxygen generation of F_2PMet, ZnF_2PMet, and phenalenone using the Stern–Volmer plot is presented in figure 3.

The same figure shows singlet molecular oxygen detected after excitation of the ZnF_2PMet. For comparison, the molecules were all excited at 355 nm, to use the same reference compound. As can be seen, Φ_Δ values are strongly affected by the substitution pattern and show the following trend: F_2PMet < ZnF_2PMet, with respective values of 0.71 and 0.99. The ca. 30% higher Φ_Δ values are obtained for ZnF_2PMet and this sensitizer acts via Type-II photochemical process almost exclusively. Coordination of the zinc ion increases Φ_Δ and decreases k_q value. This suggests that the increase in Φ_Δ is related to an increase in the triplet quantum yield, and therefore, to a heavy-atom effect. The internal heavy atom effect assists halogenated porphyrins to generate triplet states with quantum yields approaching a unity. The introduction of Zn^{2+} into tetraphenylporphyrin derivatives improves photophysical and photochemical properties influencing photodynamic activity.

3.5. *Interaction of F_2PMet and ZnF_2PMet with HSA studied by fluorescence measurements*

Metallodrug-plasma protein interactions are of considerable pharmacological importance because the efficacy of new drugs critically depends on their binding to plasma proteins. Many promising new drugs, for instance, have been rendered ineffective because of their unusually high affinity to albumin and the binding of a new drug to albumin has therefore been referred to as the "second step in rational drugs design" [54]. In this context, understanding the binding of porphyrins to plasma protein is crucial of the success of these photosensitizers being used in PDT. In this work, the ability of interaction between F_2PMet and its zinc complex (ZnF_2PMet) was studied by fluorescence quenching measurements. The fluorescence of HSA at $\lambda_{max} = 355$ nm is mainly due to amino acid (tryptophan, Trp) residues. The fluorescence emission spectra of HSA at different concentrations of ZnF_2PMet are given in figure 4 (left).

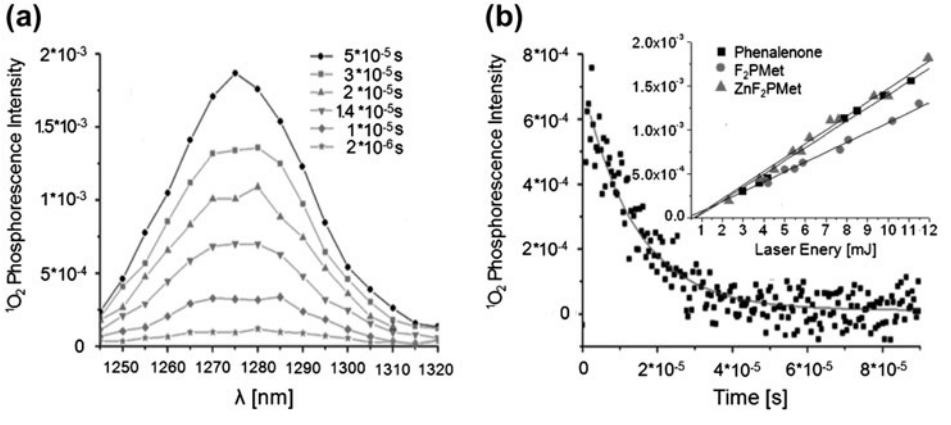

Figure 3. Singlet molecular oxygen emission spectra registered for ZnF_2PMet in ethanol (a); Emission intensity measured at 1270 nm as a function of the laser energy (b, inset) and the decay of singlet oxygen generated by ZnF_2PMet in ethanol (b).

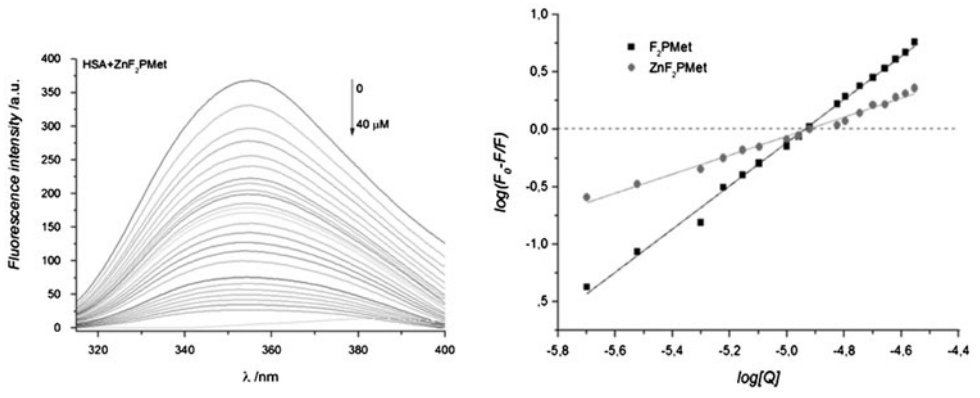

Figure 4. Fluorescence spectral changes of HSA in PBS buffer (pH 7.4) after addition of varying concentrations of ZnF_2PMet (left); Scatchard plot analysis. Binding of F_2PMet and ZnF_2PMet to HSA measured from the emission of the protein (right).
Notes: Experimental conditions: [HSA] = 5 μM; [F_2PMet], [ZnF_2PMet] = 0–40 μM; λ_{exc} = 295 nm, λ_{em} = 300–400 nm.

The addition of porphyrin to solution of HSA caused the quenching of the intrinsic protein fluorescence. Porphyrin may bind at the surface of HSA (more hydrophobic environment) and the shield from the solvent may lead to the blue shift of the HSA emission maximum. Due to mutual quenching it is possible to determine the Stern–Volmer quenching constants (K_{SV}). The slope of the plots shown in figure 4 (right) gave the K_{SV} in PBS buffer as listed in table 2 and suggests that HSA fluorescence quenching is more effective for F_2PMet than ZnF_2PMet. Moreover, the Stern–Volmer kinetics showing positive linear correlation could be also an indication that in contrast to phthalocyanines [54], the mechanism of HSA quenching by porphyrin may be diffusion-controlled (not static, but dynamic quenching).

Protein fluorescence quenching can also be used to retrieve porphyrin-HSA binding parameters. The parameters obtained from Scatchard plot analysis (K_b and number of binding sites, figure 4, table 3) are consistent with the presence of many binding sites. As can be seen in figure 4 and table 3, the K_b for F_2PMet is higher than those of ZnF_2PMet. The higher the value of this parameter, the stronger is the binding between the porphyrin and HSA. Our results indicate that these photosensitizers bind to HSA efficiently but the free-base porphyrin binds more strongly to HSA because of its more hydrophobic character. This trend in data is similar to results obtained for other porphyrin derivatives. Rinco and co-workers reported that more hydrophilic porphyrin-like hematoporphyrin IX dimethylester does not seem to bind with HSA probably due to the lack of hydrophobic sites [55]. It is suggested that the difference in HSA binding and aggregation properties of photosensitizers

Table 3. Fluorescence quenching and binding data for the interaction of HSA with F_2PMet and ZnF_2PMet.

Photosensitizer	K_{SV} (M^{-1})	K_b (M^{-1})	n
F_2PMet	8.85×10^4	1.88	>2
ZnF_2PMet	7.61×10^4	0.83	>2

may be relevant to their *in vivo* efficacy, blood transport, and biodistribution; therefore, the porphyrin-albumin system is a widely accepted model to study the behavior of this molecules in organisms.

3.6. *Time-dependent cellular uptake*

The time-dependent cellular uptake by A549 cancer cells was investigated in cells exposed to 5 μM of photosensitizer solutions. Figure 5 presents the time-dependent cellular accumulation of F_2PMet and ZnF_2PMet in A549 cells. The uptake was approximately linearly increasing with time for the first 2–6 h for ZnF_2PMet and 2–18 h for F_2PMet. The maximum amount of ZnF_2PMet in the cells was obtained after 6 h of incubation with concentration about 25 pM per cell and is about five times larger than the intracellular concentration of F_2PMet.

For free-base porphyrin, the optimal incubation time was 18 h. This significant difference can be explained by stronger interaction with biological membranes that is usually related to the larger inclusion of photosensitizer in cells. Better cellular uptake of ZnF_2PMet in comparison to F_2PMet may be also connected with physicochemical character of this compound, because the hydrophobicity of the photosensitizer is related to its interaction with biological membranes. An amphiphilic photosensitizer such as ZnF_2PMet ($\log P_{OW} = 1.72$) may traverse the bilayer either by simple diffusion or by hijacking the cell's transport system. However, one should consider that binding of zinc porphyrins to phospholipid membranes may also be determined by metal–phosphate coordination. In accordance to Pashkovskaya *et al.*, the efficacy of the metallophthalocyanines binding to bilayer lipid membranes measured by boundary potentials dependent on the central metal atom in the macrocycle ring and the affinity to the membrane is the highest for zinc complexes. Moreover, they suggested that formation of a coordination bond between Zn^{2+} and the phosphate group of phospholipids plays an essential role in photosensitizer binding to biological membranes [56].

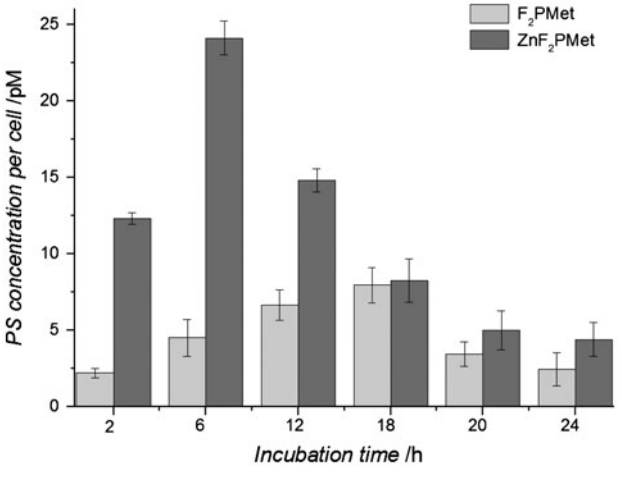

Figure 5. Time-dependent uptake of F_2PMet and ZnF_2PMet 5 μM by A549 cells as measured by fluorescence intensity.

3.7. *Dark cytotoxicity and photodynamic effect*

The cytotoxicity of F_2PMet and ZnF_2PMet against A549 cells was tested in the dark using the cell surviving MTT assay. The dark toxicity of these porphyrins was performed after 6 h and 24 h incubations (figure 6, left). The investigated photosensitizers had no effect on the viability with concentrations ranging from 0 to 25 μM. Only very high concentration of porphyrins such as 50 μM turned out to be slightly toxic to the tested cancer cells. This result also indicates that the dark cytotoxicity of ZnF_2PMet and its metal-free analog at the concentration used in photodynamic experiments (5 μM) is negligible.

In order to assess the photodynamic effect on the cells in function of irradiation time (light dose), the A549 cells were exposed for 6 h to F_2PMet and ZnF_2PMet at concentration 5 μM and then irradiated with red light (ca. λ ~600 nm) with irradiation times from 0 to 60 min. The dependence of cell viability on the irradiation time is shown in figure 6. Both F_2PMet and ZnF_2PMet induced cell death increased in efficacy as a total light dose increased from 0 to 6 J cm^{-2}. The drop in surviving fraction was steep even at short irradiation times and the trend in cell response is similar in both cases. However, F_2PMet demonstrated a stronger PDT effect than ZnF_2PMet and when the metal-free porphyrin was used as photosensitizer A549 cells are most sensitive reaching a 70% mortality (6 J cm^{-2}), in contrast to ZnF_2PMet with surviving fraction at 58%. Note that a decrease in cell surviving fraction and a consequent increase in photodynamic activity do not parallel the increase in uptake by the cells (figure 6, right). Thus, other factors than intracellular accumulation of photosensitizer must explain the lower PDT efficacy of ZnF_2PMet compared with the unsubstituted analog porphyrin. This unusual relationship between porphyrin cellular uptake and phototoxicity is expected considering that F_2PMet shows lower singlet oxygen generation quantum yields ($\Phi_\Delta = 0.71$) and increase in free radical formation by charge transfer processes (type-I mechanism). Efficient hydroxyl radical formation is usually related with improved PDT activity. Literature data indicate that Zn-photosensitizers have better efficiency compared with their metal-free derivatives [53]. Our approach stands in contrast to these findings, but we are able to explain that it is the tendency, but not the rule, and it strongly depends on electronic structure, photophysical, and electrochemical properties of

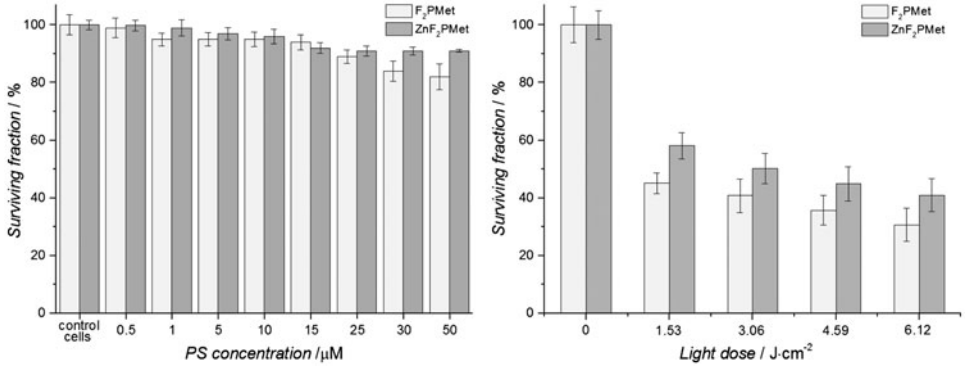

Figure 6. Cytotoxicity in the dark of F_2PMet and ZnF_2PMet tested against A549 cells (left) and photodynamic effect after 6 h incubation A549 cells with F_2PMet or ZnF_2PMet (right).
Notes: The cells were irradiated with ~600 nm LED light for various time intervals and their availability was determined by MTT assay.

photosensitizer and show that is due to the favorable type-I of photoreaction mechanism. Therefore, the mechanism of ROS generation by photosensitizer seems to be the major factor affecting the highest phototoxicity for A549 cells.

3.8. *Subcellular localization*

Confocal microscopy was used to determine the subcellular localization of F_2PMet by overlapping the fluorescence image of the photosensitizer with specific organelle trackers for ER, mitochondria, and lysosome. ZnF_2PMet is diffused all over the cell (figure 7) and bonded to membrane proteins.

In contrast, the fluorescence micrographs obtained for F_2PMet reveal a diffuse pattern of porphyrin localization through the cytoplasm with a more intense fluorescence in the perinuclear area of the cell. The red fluorescence of this photosensitizer is distributed through the entire cytoplasm and remains outside the nucleus. According to the topographic analysis their localization is more coincident with the ER and mitochondria while overlapping with the lyso-tracker is almost nonexistent (figure 8). Taking into account the high affinity of F_2PMet to interact with cell membranes and to be localized in a lipid environment, binding to Golgi apparatus should not be excluded. There is a substantial knowledge on the PDT effect of different sub-cellular localizations of various porphyrins and related compounds such as phthalocyanines. Photosensitizers that localize in mitochondria are known to be more phototoxic than ones localized in lysosomes [35, 36]. Baptista *et al.* have reported that zinc-porphyrin derivatives have higher cellular uptakes than metal-free porphyrins [57]. On the other hand, zinc insertion decreased the interaction with mitochondria and increased membrane interaction. Thus, Zn complexes have the lowest mitochondrial uptake and the highest cell uptake, indicating that this molecule tends to accumulate unspecifically in phospholipid bilayers instead of concentrating in mitochondria. Binding seems to be affected mainly by the hydrophobic effect and the electrostatic component.

Therefore, addition of zinc increases the hydrophilic character of these porphyrins and decreases the hydrophobic interaction with the membranes. Another possibility to explain the stronger binding of free-base porphyrins compared to zinc porphyrins would be that free-base porphyrins can get chelated in biological media by free or partially chelated metals, i.e. they could get chelated in the mitochondria increasing its binding efficiency.

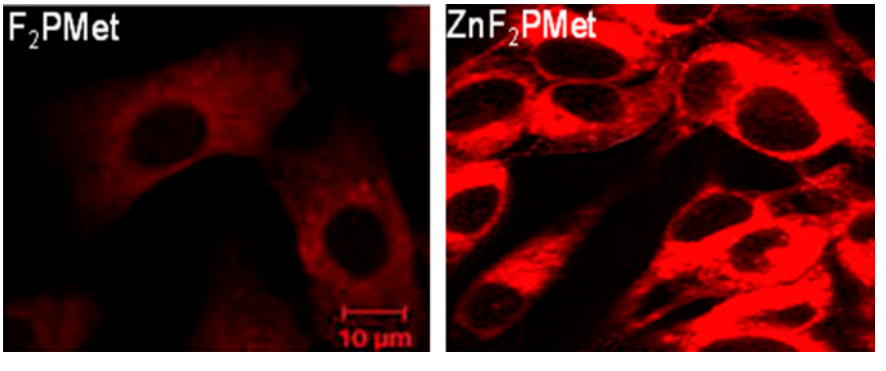

Figure 7. Intracellular distribution of F_2PMet (left) and ZnF_2PMet (right) in A549 cells.

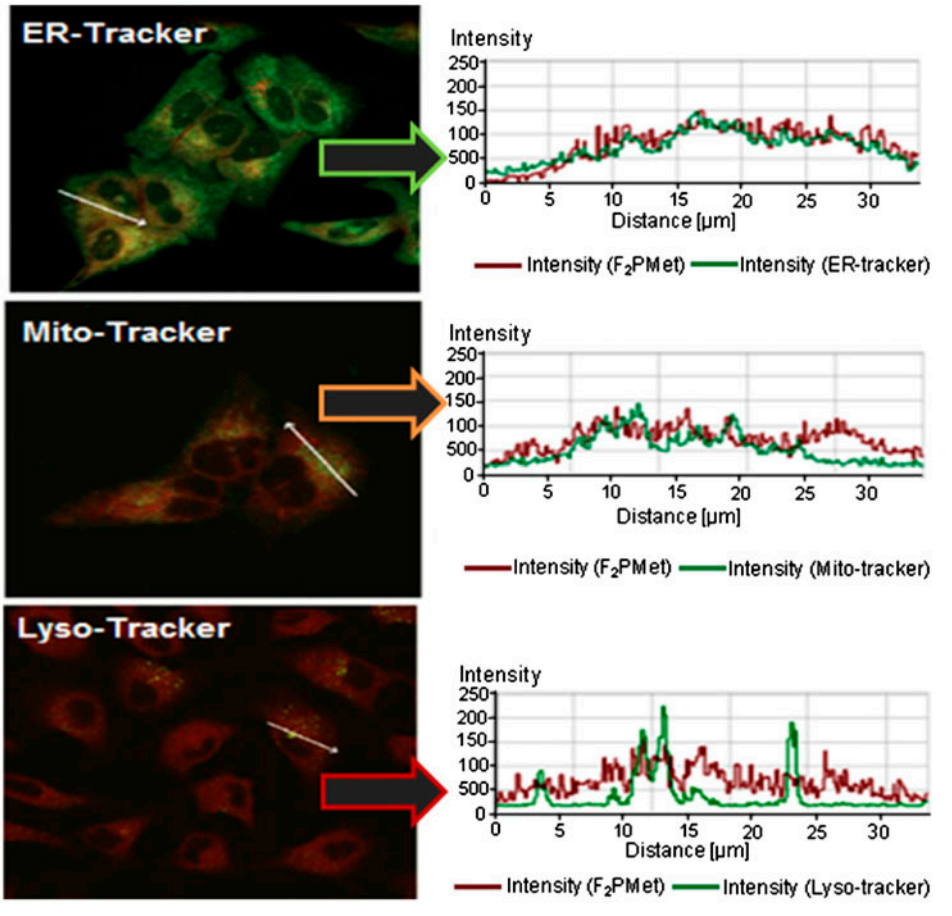

Figure 8. Fluorescence micrographs of A549 cells showing intracellular localization of F_2PMet evaluated by confocal microscopy.
Notes: Cells were marked with dyes for ER (ER-Tracker), lysosomes (Lyso-Tracker), and mitochondria (Mito-Tracker). For each image, a profile of fluorescence intensity along the white arrow is shown. The green topographic profile corresponds to the emission of the tracker and the red to the porphyrin emission.

Pavani *et al.* also indicate that photosensitizers chelated with zinc have a lower tendency to accumulate in mitochondria but present higher efficiency in damaging this organelle, leading to a higher percentage of cells engaging in apoptotic cell death. Free-base porphyrins, which have higher accumulation in mitochondria, cause a rapid loss of membrane integrity, favoring a necrotic route of cell death [53, 57].

3.9. *ROS generation*

The balance between type-II (energy transfer and singlet oxygen generation) and type-I (charge transfer processes with free radical formation) photochemical mechanisms is thought to play an important role in the specific PDT activity of tetrapyrrolic photosensitizers. The propensities of F_2PMet and ZnF_2PMet to generate ROS via type-I *versus* type-II

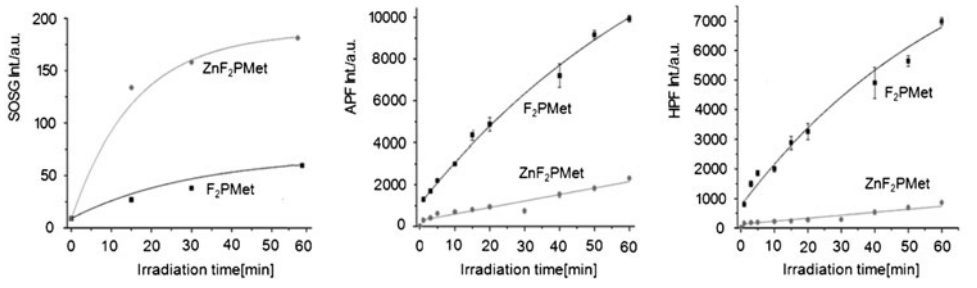

Figure 9. ROS generation. Fluorescence generated from ROS probes in solution (10 μM): (1) SOSG; (2) 3′-(*p*-aminophenyl)fluorescein (APF); (3) 3′-(*p*-hydroxyphenyl)fluorescein (HPF). The porphyrins were directly diluted to a final concentration of 5 μM per well in phosphate-buffered saline and excited with red light.

mechanisms were assessed using fluorescence probes (SOSG, APF, and HPF) that have been reported to be relatively specific for the two most important ROS in PDT-induced cell death: singlet oxygen and hydroxyl radical (figure 9). Although F_2PMet produces singlet oxygen and hydroxyl radicals, the balance between these two mechanisms definitely favors type-I photochemistry. The least active photosensitizer, ZnF_2PMet, has significantly lower ratios of APF and HPF in comparison to SOSG activation and therefore acts more via type-II than type-I photochemistry. It could not have been anticipated that a free base species produces more hydroxyl radicals than a zinc chelate, a conclusion that is at least true for the photosensitizers investigated in this work. In summary, the comparison between F_2PMet and ZnF_2PMet shows that greater PDT activity toward A549 cells correlates with greater propensity for type-I photochemistry, namely hydroxyl radical formation.

4. Conclusion

We have compared the spectroscopic and photochemical properties of free and Zn-substituted halogenated amphiphilic porphyrins. Zinc insertion into the porphyrin ring changes the hydrophobicity, cellular localization, and the final photodynamic efficiency *in vitro*. The presence of zinc decreases hydrophobicity, increases cellular uptake, but does not lead to improved PDT efficiency although the singlet oxygen quantum yield of Zn-porphyrin is higher than that of the free-base analog. The free-base porphyrin is localized more specifically in critical biological targets such as mitochondria and endoplasmatic reticulum and generates both singlet oxygen and hydroxyl radicals. The photodynamic efficiency in A549 cells seems to be more closely related with the photogeneration of hydroxyl radicals than the accumulation of photosensitizer in the cells, suggesting that having a favorable photochemical mechanism is a key factor to achieve an improved photodynamic effect.

Acknowledgements

We also thank Luzitin SA for supplying some compounds and Luisa Cortes for the assistance in confocal microscopy experiments.

Disclosure statement

No potential conflict of interest was reported by the authors.

Funding

This work was funded by Ministry of Science and Higher Education within the Iuventus Plus programme [grant number 0085/IP3/2015/73]. We also thank National Science Centre for [grant number 2012/05/BST5/00389], [grant number 2013/11/D/ST5/02995]. MMP and LGA thank FCT and FEDER for [grant number PEst-OE/QUI/UI0313/2014], [grant number UID/QUI/00313/2013]. The Faculty of Chemistry of the Jagiellonian University is the beneficiary of the structural funds from the European Union [grant number POIG. 02.01.00-12-023/08].

References

[1] J.M. Dabrowski, L.G. Arnaut. *Photochem. Photobiol. Sci.*, (2015). doi:10.1039/c5 pp00132c.
[2] L. Huang, M. Krayer, J.G.S. Roubil, Y.Y. Huang, D. Holten, J.S. Lindsey, M.R. Hamblin. *J. Photochem. Photobiol., B*, **141**, 119 (2014).
[3] T. Zoltan, F. Vargas, V. López, V. Chávez, C. Rivas, Á.H. Ramírez. *Spectrochim. Acta, Part A*, **135**, 747 (2015).
[4] M. Ethirajan, Y. Chen, P. Joshi, R.K. Pandey. *Chem. Soc. Rev.*, **40**, 340 (2011).
[5] M.G.H. Vicente. *Curr. Med. Chem. Anti-cancer Agents*, **1**, 175 (2001).
[6] J.M. Dąbrowski, M.M. Pereira, L.G. Arnaut, C.J.P. Monteiro, A.F. Peixoto, A. Karocki, K. Urbańska, G. Stochel. *Photochem. Photobiol.*, **83**, 897 (2007).
[7] A.V.C. Simões, A. Adamowicz, J.M. Dąbrowski, M.J.F. Calvete, A.R. Abreu, G. Stochel, L.G. Arnaut, M.M. Pereira. *Tetrahedron*, **68**, 8767 (2012).
[8] M. Kempa, P. Kozub, J. Kimball, M. Rojkiewicz, P. Kuś, Z. Gryczyński, A. Ratuszna. *Spectrochim. Acta, Part A*, **146**, 249 (2015).
[9] E.F.F. Silva, F.A. Schaberle, C.J.P. Monteiro, J.M. Dąbrowski, L.G. Arnaut. *Photochem. Photobiol. Sci.*, **12**, 1187 (2013).
[10] J.A. Hargus, F.R. Fronczek, M.G.H. Vicente, K.M. Smith. *Photochem. Photobiol.*, **83**, 1006 (2007).
[11] A. Szurko, M. Rams, A. Sochanik, K. Sieroń-Stołtny, A.M. Kozielec, F.P. Montforts, R. Wrzalik, A. Ratuszna. *Bioorg. Med. Chem.*, **17**, 8197 (2009).
[12] J.M. Dąbrowski, L.G. Arnaut, M.M. Pereira, C.J.P. Monteiro, K. Urbańska, S. Simões, G. Stochel. *ChemMedChem*, **5**, 1770 (2010).
[13] J.M. Dąbrowski, M. Krzykawska, L.G. Arnaut, M.M. Pereira, C.J.P. Monteiro, S. Simões, K. Urbańska, G. Stochel. *ChemMedChem*, **6**, 1715 (2011).
[14] L.G. Arnaut, M.M. Pereira, J.M. Dąbrowski, E.F.F. Silva, F.A. Schaberle, A.A. Abreu, L.B. Rocha, M.M. Barsan, K. Urbańska, G. Stochel, C.M.A. Brett. *Chem. Eur. J.*, **20**, 5346 (2014).
[15] Y.Y. Huang, T. Balasubramanian, E. Yang, D. Luo, J.R. Diers, D.F. Bocian, J.S. Lindsey, D. Holten, M.R. Hamblin. *ChemMedChem*, **7**, 2155 (2012).
[16] J.M. Dąbrowski, K. Urbanska, L.G. Arnaut, M.M. Pereira, A.R. Abreu, S. Simões, G. Stochel. *ChemMedChem*, **6**, 465 (2011).
[17] J.M. Dąbrowski, L.G. Arnaut, M.M. Pereira, K. Urbańska, G. Stochel. *MedChemComm*, **3**, 502 (2012).
[18] R. Saavedra, L.B. Rocha, J.M. Dąbrowski, L.G. Arnaut. *ChemMedChem*, **9**, 390 (2014).
[19] Y.Y. Huang, P. Mroz, T. Zhiyentayev, S.K. Sharma, T. Balasubramanian, C. Ruzié, M. Krayer, D. Fan, K.E. Borbas, E. Yang, H.L. Kee, C. Kirmaier, J.R. Diers, D.F. Bocian, D. Holten, J.S. Lindsey, M.R. Hamblin. *J. Med. Chem.*, **53**, 4018 (2010).
[20] M. Krzykawska-Serda, J.M. Dąbrowski, L.G. Arnaut, M. Szczygieł, K. Urbańska, G. Stochel. *Free Radical Biol. Med.*, **73**, 239 (2014).
[21] L.B. Rocha, L. Gomes-da-Silva, J.M. Dąbrowski, L.G. Arnaut. *Eur. J. Cancer* (2015). doi:10.1016/j.ejca.2015.06.002.
[22] S.V. Dudkin, E.A. Makarova, L.K. Slivka, E.A. Lukyanets. *J. Porphyrins Phthalocyanines*, **18**, 107 (2014).
[23] A.D. Quartarolo, D. Pérusse, F. Dumoulin, N. Russo, E. Sicilia. *J. Porphyrins Phthalocyanines*, **17**, 980 (2013).
[24] D. Lafont, Y. Zorlu, H. Savoie, F. Albrieux, V. Ahsen, R.W. Boyle, F. Dumoulin. *Photodiagn. Photodyn. Ther.*, **10**, 252 (2013).
[25] B.G. Ongarora, X. Hu, H. Li, F.R. Fronczek, M.G.H. Vicente. *Med. Chem. Commun.*, **3**, 179 (2012).
[26] W. Liu, T.J. Jensen, F.R. Fronczek, R.P. Hammer, K.M. Smith, M.G.H. Vicente. *J. Med. Chem.*, **48**, 1033 (2005).
[27] K. Szaciłowski, W. Macyk, A. Drzewiecka-Matuszek, M. Brindell, G. Stochel. *Chem. Rev.*, **105**, 2647 (2005).

[28] Y. Vakrat-Haglili, L. Weiner, V. Brumfeld, A. Brandis, Y. Salomon, B. Mcllroy, B.C. Wilson, A. Pawlak, M. Rozanowska, T. Sarna, A. Scherz. *J. Am. Chem. Soc.*, **127**, 6487 (2005).
[29] E.F.F. Silva, C. Serpa, J.M. Dąbrowski, C.J.P. Monteiro, L.G. Arnaut, S.J. Formosinho, G. Stochel, K. Urbanska, S. Simoes, M.M. Pereira. *Chem. Eur. J.*, **16**, 9273 (2010).
[30] J.M. Dąbrowski, L.G. Arnaut, M.M. Pereira, K. Urbanska, S. Simoes, G. Stochel, L. Cortes. *Free Radical Biol. Med.*, **52**, 1188 (2012).
[31] P.R. Ogilby. *Photochem. Photobiol. Sci.*, **9**, 1543 (2010).
[32] D. Kessel, Y. Luo, Y. Deng, C.K. Chang. *Photochem. Photobiol.*, **65**, 422 (1997).
[33] H. Mojzisova, S. Bonneau, C. Vever-Bizet, D. Brault. *Biochim. Biophys. Acta (BBA) – Biomembr.*, **1768**, 2748 (2007).
[34] K. Berg, A. Western, J.C. Bommer, J. Moan. *Photochem. Photobiol.*, **52**, 481 (1990).
[35] N.L. Oleinick, R.L. Morris, I. Belichenko. *Photochem. Photobiol. Sci.*, **1**, 1 (2002).
[36] T.I. Peng, C.J. Chang, M.J. Guo, Y.H. Wang, J.S. Yu, H.Y. Wu, M.J. Jou. *Ann. NY. Acad. Sci.*, **1042**, 419 (2005).
[37] L. Benov. *Med. Princ. Pract.*, **24**, 14 (2015).
[38] P. Mroz, J. Bhaumik, D.K. Dogutan, Z. Aly, Z. Kamal, L. Khalid, H.L. Kee, D.F. Bocian, D. Holten, J.S. Lindsey, M.R. Hamblin. *Cancer Lett.*, **282**, 63 (2009).
[39] J. Cao, D.C. Hu, J.C. Liu, R.Z. Li, N.Z. Jin. *J. Coord. Chem.*, **66**, 421 (2013).
[40] N. Hessenauer-Ilicheva, A. Franke, D. Meyer, W.D. Woggon, R. van Eldik. *Chem. Eur. J.*, **15**, 2941 (2009).
[41] C.D. Hubbard, R. van Eldik. *J. Coord. Chem.*, **60**, 1 (2007).
[42] A.S. Sobolev, D.A. Jans, A.A. Rosenkranz. *Prog. Biophys. Mol. Biol.*, **73**, 51 (2000).
[43] B.L. Wheeler, G. Nagasubramanian, A.J. Bard, L.A. Schechtman, D.R. Dininny, M.E. Kenney. *J. Am. Chem. Soc.*, **106**, 7404 (1984).
[44] N. Kobayashi, H. Ogata, N. Nonaka, E.A. Lukyanets. *Chem. Eur. J.*, **9**, 5123 (2003).
[45] M. Durmuş, V. Ahsen, T. Nyokong. *J. Photochem. Photobiol., A*, **186**, 323 (2007).
[46] A.M.A.R. Gonsalves, J.M.T.B. Varejão, M.M. Pereira. *J. Heterocycl. Chem.*, **28**, 635 (1991).
[47] M. Silva, A. Fernandes, S.S. Bebiano, M.J.F. Calvete, M.F. Ribeiro, H.D. Burrows, M.M. Pereira. *Chem. Commun.*, **50**, 6571 (2014).
[48] A.D. Adler, F.R. Longo, F. Kampas, J. Kim. *J. Inorg. Nucl. Chem.*, **32**, 2443 (1970).
[49] R. Schmidt, C. Tanielian, R. Dunsbach, C. Wolff. *J. Photochem. Photobiol., A*, **79**, 11 (1994).
[50] L.G. Arnaut. *Adv. Inorg. Chem.*, **63**, 187 (2011).
[51] D. Kessel, K.M. Smith, R.K. Pandey. *Photochem. Photobiol.*, **58**, 200 (1993).
[52] M.M. Pereira, C.J.P. Monteiro, A.V.C. Simões, S.M.A. Pinto, A.R. Abreu, G.F.F. Sá, E.F.F. Silva, L.B. Rocha, J.M. Dąbrowski, S.J. Formosinho, S. Simões, L.G. Arnaut. *Tetrahedron*, **66**, 9545 (2010).
[53] C. Pavani, A.F. Uchoa, C.S. Oliveira, Y. Iamamoto, M.S. Baptista. *Photochem. Photobiol. Sci.*, **8**, 233 (2009).
[54] S. Tuncel, F. Dumoulin, J. Gailer, M. Sooriyaarachchi, D. Atilla, M. Durmuş, D. Bouchu, H. Savoie, R.W. Boyle, V. Ahsen. *Dalton Trans*., **40**, 4067 (2011).
[55] O. Rinco, J. Brenton, A. Douglas, A. Maxwell, M. Henderson, K. Indrelie, J. Wessels, J. Widin. *J. Photochem. Photobiol., A*, **208**, 91 (2009).
[56] A.A. Pashkovskaya, E.A. Sokolenko, V.S. Sokolov, E.A. Kotova, Y.N. Antonenko. *Biochim. Biophys. Acta (BBA) – Biomembr.*, **1768**, 2459 (2007).
[57] C. Pavani, Y. Iamamoto, M.S. Baptista. *Photochem. Photobiol.*, **88**, 774 (2012).